# Modelling of Flow Characteristics of Main Rotor with Elliptical Root Section in Hover Mode

*Sergey* Kusyumov[1,*], *Robert* Stepanov[1], *Alexander* Kusyumov[1], *Ruslan* Mirgazov[2], and *Boris* Kritsky[2]

[1]Kazan National Research Technical University, Kazan, Russia
[2]Zhukovsky Central Aerohydrodynamics Institute (TsAGI)

**Abstract.** The modelling of a helicopter main rotor flow field in hover regime is being considered. The aerodynamic and aeroacoustics characteristics of two rotor models with different blade root geometries are compared. The first rotor has the shape of NACA0012 air foil in the root section of the blades. The second rotor model has an elliptic air foil in the root of the rotor blade. The amplitude and temporal characteristics of the aeroacoustics emission in near-field are investigated using Computational Fluid Dynamics (CFD).

## 1 Introduction

In recent years a growing number of publications has been dedicated to numerical modelling of various helicopter applications, such as rotor aerodynamics in hover and forward flight [1], the acoustic field generated by a helicopter rotor [2], and the comparison of aeroacoustics data obtained from numerical simulations of a helicopter rotor in hover with near-field experimental data [3].

The design of modern high-speed helicopters imposes specific requirements to the blade geometry of the main rotor. High-speed helicopter flight is characterized by a reverse flow region near the root section of the rotor blade. In such conditions, the resulting flow is directed from the trailing edge to the leading edge of the blade. The use of conventional air foils with sharp trailing edge (similar to NACA0012) in such conditions has a negative effect on the thrust and vibrations of the rotor. A possible solution to this problem is to use a "non-conventional" air foil at the root section of the rotor blade. A low separation, double-ended blunt-edge DBLN526 air foil was used in order to handle this problem during the design of X2TD Sikorsky demonstrator [4].

In this work, the influence of an elliptic DBLN526 air foil in the root section of the blade on the aerodynamic and aeroacoustics characteristics of a rotor in hover mode is considered and compared with the conventional NACA0012 air foil. The amplitude and temporal characteristics of aeroacoustics emission in near-field are investigated using Computational Fluid Dynamics (CFD).

The numerically obtained results (VMB solver, the University of Glasgow and KNRTU-KAI) of integral aerodynamic characteristics of the rotor are compared to experimental data,

* Corresponding author: kusok88@yandex.ru

obtained in T-1K wind tunnel at KNRTU-KAI. In order to reduce the volume of the modelling domain in hover regime, the boundary conditions are obtained using "source–sink" model (ideal fluid).

## 2 Problem formulation for numerical simulation

During the hovering regime, the flow field is symmetric (periodic). Therefore, the modeling is carried out for a single blade, for the azimuth angles ranging from $0^{\circ}$ to $90^{\circ}$.

The modeling was carried out for two rotors. The first main rotor, denoted as R1 (model of Laboratory 1 at KNRTU-KAI), had a constant (baseline) airfoil shape along the blade span. The second rotor, denoted as R2, had an elliptic blade root shape of DBLN526 airfoil. The airfoil geometry of the second rotor remained constant starting from the root section $\bar{r}_0$ up to $\bar{r}_1$ section, as shown in Figure 1. The blade geometry morphed continuously from DBLN526 airfoil at $\bar{r}_1$ into NACA0012 airfoil at $\bar{r}_2$ and did not change up to $\bar{r} = 1$. Here $\bar{r} = r/R$ is the non-dimensional radius of the blade relative of the rotor radius $R$. The blade was spanning from $\bar{r} = 0.2$ to $\bar{r} = 1$.

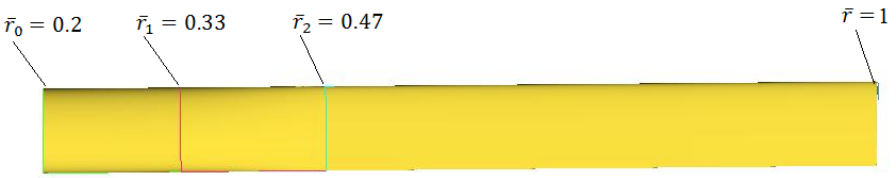


**Fig. 1.** The planform of the R1 and R2 rotor blades.

The NACA0012 airfoil was chosen as the baseline airfoil. The DBLN526 airfoil (26% thickness, and 4% camber) was also used in R2 rotor model. The comparison of NACA0012 and the DBLN526 airfoil geometries is shown in Figure 2.

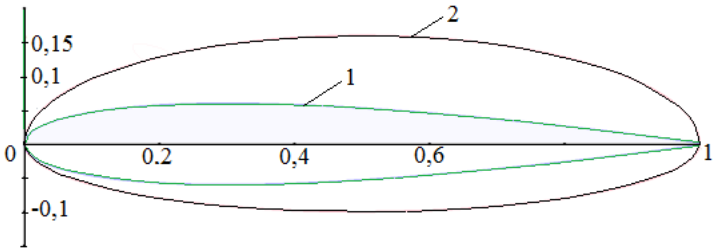


**Fig. 2.** The comparison of the airfoil geometries in the root of the rotor blade: (1) NACA0012 airfoil; (2) DBLN526 airfoil.

Main geometric parameters of the rotors are given in Table 1.

**Table 1.** Geometric parameters of R1 and R2 rotor models.

| **Parameters** | **Value** | |
|---|---|---|
| **Rotor model** | **R1** | **R2** |
| Collective pitch angle, $\varphi_7$° | 8 | 8 |
| Number of blades, N | 4 | 4 |
| Diameter, D=2R (m) | 1.6 | 1.6 |
| Blade twist | no | no |
| Airfoil type at $\bar{r}_0 = 0.2$ | NACA0012 | DBLN526 |

| | | |
|---|---|---|
| Airfoil type at $\bar{r}_1 = 0.33$ | NACA0012 | DBLN526 |
| Airfoil type at $\bar{r}_2 = 0.47$ | NACA0012 | NACA0012 |
| Airfoil chord length, c (mm) | 65 | 65 |
| Blade tip shape | rectangular | rectangular |

Computational hexa-grids for a single rotor blade contained 88 blocks and close to 10 million of elements. The "source–sink" [5] type of boundary models was used at the upper and lower boundaries of the computational domain. The computations were carried out for the angular speeds of 900, 1400 and 2600 rpm.

The CFD modeling was carried out using the helicopter multi-block VMB solver (which is a version of Glasgow University HMB 2.0 solver adapted for KNRTU-KAI). The discretization of the Navier-Stokes equations was performed using the finite volume approach. Discretization of the convective terms was carried out using the scheme outlined in [6] and MUSCL interpolation of variables to ensure the third-order of accuracy.

## 3 Characteristics of R1 and R2 rotor models

Integral and distributed characteristics of R1 and R2 rotor models were obtained at the rotational speeds of 900 and 1400 rpm. Figure 3 shows the visualization of the tip vortex trajectory using Q-criterion [7].

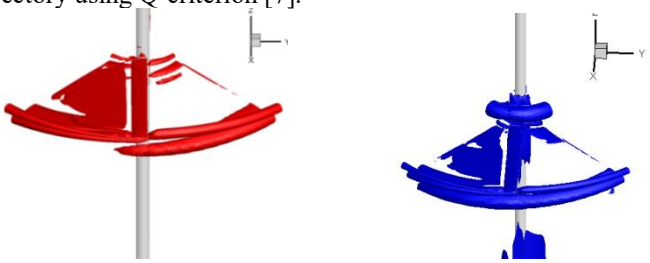

(a) (b)

**Fig. 3.** Visualization of the tip vortex trajectory using Q-criterion (Q=0.001) at the rotational speed of 1400 rmp: (a) R1 rotor; (b) R2 rotor.

As shown in Figure 3, the change of the root geometry of the rotor blade does not significantly affect the trajectory of the tip vortex at the considered rotational speed in hover regime. The acoustic pressure distribution $dP = p - p_\infty$ on the rotor plane of rotation is shown in Figure 4. Here $p$ is the local pressure and $p_\infty$ is the reference (atmospheric) pressure.

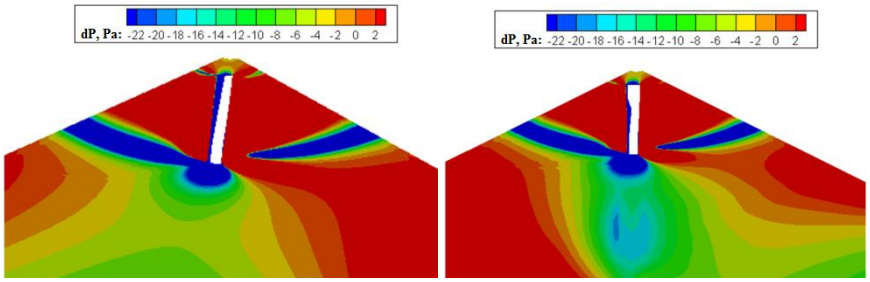


R1 R2

**Fig. 4.** The pressure distribution on the plane of rotation of R1 and R2 rotors at the rotational speed of 1400 rpm.

The presented results indicate that there is a low-pressure region (suction) in the vicinity of the blade tip and in the wake of the blade. At the same time, the low-pressure region in the wake persists for almost an entire rotor revolution. In general, the low-pressure region of R2 rotor can be observed not only in the proximity of the blade tip region, but also at farther distances (up to two radii of the blade).

Thus, a change of the root blade geometry affects, to a certain extent, the pressure distribution for practically the entire flow region in the vicinity of the blade.

The integral and aerodynamic characteristics of R1 and R2 rotors are presented in Table 2. The integral characteristics are obtained as

$$C_T = \frac{2T}{\pi\rho\omega^2 R^4}, FM = \frac{C_T^{3/2}}{2C_Q}. \quad (1)$$

Here, $C_T$ is the rotor thrust coefficient, ρ is the air density, ω is the angular velocity, $R$ is the rotor radius, $C_Q$ is the torque coefficient, and $FM$ is the figure of merit of the rotor. The experimental data for the R1 rotor was obtained in T-1K wind tunnel at KNRTU [8].

**Table 2.** Aerodynamics characteristics of R1 and R2 rotor models.

| Angular velocity, rpm | Rotor | | | | | |
|---|---|---|---|---|---|---|
| | R1(CFD) | | R2(CFD) | | R1 (Experiment) | |
| | $C_T$ | $FM$ | $C_T$ | $FM$ | $C_T$ | $FM$ |
| 900 | 0.0095 | 0.467 | 0.0101 | 0.453 | 0.012 | - |
| 1400 | 0.0103 | 0.478 | 0.0103 | 0.466 | 0.013 | - |
| 2600 | 0.011 | 0.502 | 0.0109 | 0.498 | - | - |

As shown in Table 2, the numerical modeling results for R1 rotor are slightly lower compared to the experimental data. The difference of the thrust coefficient values between the rotor's angular velocity of 900 and 1400 rpm of the numerical modeling are similar to experimental data for R1 rotor. The R2 rotor's thrust coefficient is considerably lower compared to the thrust coefficient of R1 rotor. At the same time, the figure of merit of R1 rotor is slightly higher compared to the R2 rotor. A small discrepancy of integral characteristics can be observed between the rotors at high rotational speeds.

The acoustic signal (pressure) in temporal domain is shown in Figure 5 for R1 rotor. The results of numerical modeling are compared to the experimental data at the rotational speed of 900 rpm for the observer (microphone) located on the plane of rotation at the distance of 1.2R away from the rotational axis. Reference [9] contains additional cases, where the observer is located lower and higher relative to the rotor's plane of rotation.

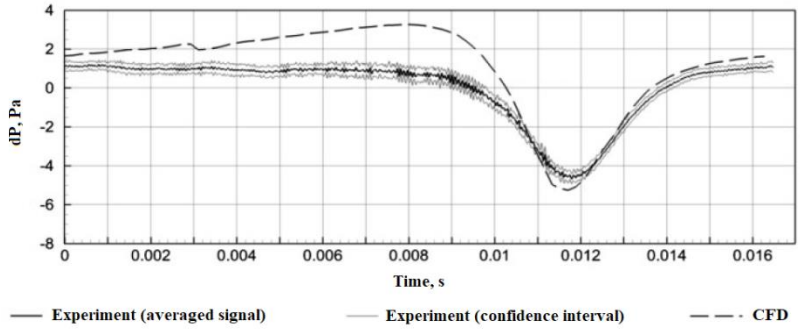


**Fig. 5.** Comparison of near-field acoustic field results.

Figure 5 and the results of reference [7] suggest that agreement between numerical modeling results and experimental data is achieved for R1 rotor at the rotational speed of 900

rpm. The aeroacoustic emission of R2 rotor at the rotational speed of 900 rpm differs insignificantly from R1 rotor. The pressure distribution of R1 and R2 rotors, obtained at other rotational speeds, are shown in Figure 6.

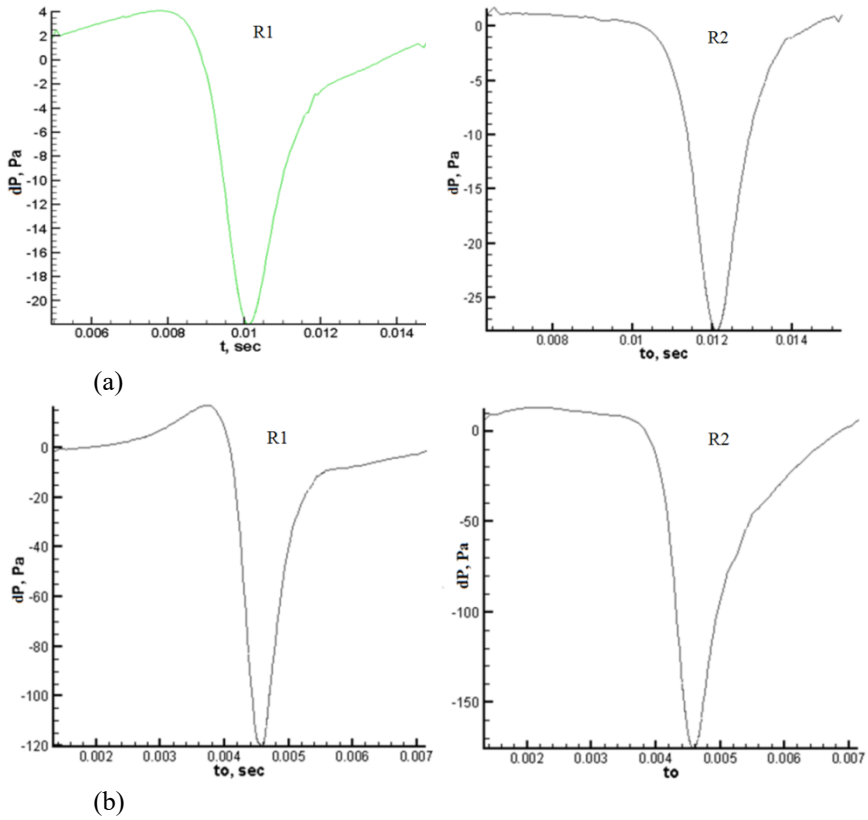


**Fig. 6.** The acoustic pressure signal for R1 and R2 rotors at different rotational speeds: (a) 1400 rpm; (b) 2600 rpm. The observer is located on the rotor plane of rotation at the distance of 1.2R away from the rotational axis.

The amplitude of the acoustic signal of R2 rotor is approximately 25% higher compared to R1 rotor in the considered rotational speed values of the rotor. Furthermore, the shape of the signal also changes: there is practically nonexistent region of the positive pressure extremum in the vicinity of the leading edge of the R2 rotor (contrary to R1 rotor).

## 4 Conclusion

The numerical modelling of main rotor flow fields was carried out using VMB CFD solver. Two rotor models were investigated: a rotor model with baseline NACA0012 air foil and the rotor with the modified root section of the blade using an elliptic air foil. The computations were performed for the hover regime.

The root shape of the blade has almost negligible impact on the integral characteristics of the rotor (the thrust coefficient and the figure of merit) at high angular speeds of the rotor.

For the observer, located in the near-field of the rotational plane of the rotor, the amplitude signal (the “peak to peak” value) depends considerably on the rotor’s angular speed, and on the root shape of the blade. The elliptic root shape of the rotor blade leads to 25% increase

of the acoustic signal amplitude compared to the baseline rotor (with baseline air foil) for high rotational speed values of the rotor.

This work was supported by the grant "FZSU-2023-0005" (No. 123030100016-5) of the Ministry of Education and Science of the Russian Federation.

## References

1. Y. Ignatkin, P. Makeev, S. Konstantinov, A. Shomov, Modelling the helicopter rotor aerodynamics at forward flight with free wake model and URANS method. Aviation, **24**, 149–15 (2020) doi: 10.3846/aviation.2020.12714.
2. I. Abalakin, P. Bahvalov, V. Bobkov, T. Kozubskaya, V. Anikin, Numerical simulation of aerodynamic and acoustic characteristics of a ducted rotor, Math. Models Comput. Simul., **8**, 309–324 (2016) doi: 8:309-324. 10.1134/S2070048216030030.
3. V. Kopiev, M. Zaytsev, V. Vorontsov, S. Karabasov, V. Anikin, Helicopter noise in hover: Computational modelling and experimental validation, Acoust. Phys., **63**, 686–698 (2017) doi: 63. 686-698. 10.1134/S1063771017060070.
4. Y. Xudong, H. Ming, Aerodynamic Design of a Rigid Coaxial Rotor Airfoil in Unsteady Flow. The 31st Congress of the Int. Council of the Aeronautical Sci., Belo Horizonte, Brazil. Sept. 9–14 (2018)
5. N.A. Mohd, G.N. Barakos, Computational aerodynamics of hovering helicopter rotors. RAeS Aerodynamics Conf., University of Bristol. UK. July 27–28 (2010)
6. B. Van Leer, Flux-vector splitting for the Euler equations. Lecture notes in physics, **170**, 507–512 (1982) doi: 10.1007/3-540-11948-5_66
7. J. Jeong, F. Hussain, On the identification of a vortex, J. of Flu. Mech., **1**, 69–94 (1995) doi: doi.org/10.1017/S0022112095000462
8. V. Pakhov, K. Fayzullin, S. Denisov, Measuring the Acoustic Characteristics of a Helicopter Rotormodel in a Wind Tunnel, Acoust. Phys., **66**, 44–54 (2020) 10.1134/S1063771020010078
9. R. Stepanov, V. Pakhov, A. Bozhenko, A. Batrakov, L. Garipova, A. Kusyumov, S. Mikhaylov, G. Barakos, Experimental and numerical study of rotor aeroacoustics. Int. J. Aeroacoustics, **16**(6), 460–475 (2017) doi: /doi.org/10.1177/1475472X1773